Phase stability and transformations in the halide perovskite CsSnI$_3$

E. Lora da Silva, Jonathan M. Skelton, Stephen C. Parker, and Aron Walsh[*]

Department of Chemistry, University of Bath, Bath, United Kingdom

(Received 27 February 2015; published 17 April 2015)

We employ the quasiharmonic approximation to study the temperature-dependent lattice dynamics of the four different phases of cesium tin iodide (CsSnI$_3$). Within this framework, we obtain the temperature dependence of a number of structural properties, including the cell volume, bulk modulus, and Grüneisen parameter. The Gibbs free energy of each phase is compared against the temperature-dependent Helmholtz energy obtained from the equilibrium structure within the harmonic approximation. We find that the black tetragonal perovskite phase is not dynamically stable up to at least 500 K, with the phonon dispersion displaying negative optic modes, which pass through all of the high-symmetry wave vectors in the Brillouin zone. The main contributions to the negative modes are found to be motions of the Cs atom inside the perovskite cage. The black cubic perovskite structure shows a zone-boundary instability, indicated by soft modes at the special **q** points M and R. These modes are present in calculations at the equilibrium (0 K) lattice constant, while at finite temperature additional negative modes develop at the zone center, indicating a ferroelectric instability. The yellow crystal, composed of one-dimensional (SnI$_6$)$_n$ double chains, has the same heat of formation as the orthorhombic perovskite phase at 0 K, but becomes less energetically favorable at higher temperatures, due to its higher free energy.

PACS number(s): 63.20.D−, 63.20.Ry, 63.70.+h

I. INTRODUCTION

CsSnI$_3$ belongs to the perovskite family of materials with the chemical formula ABX_3 (A = Cs, B = Sn, and X = I). This material undergoes a number of temperature-dependent phase changes [1], corresponding mostly to rotations and distortions of the perovskite octahedral cage formed by the Sn-I bonding environment. Such distortions include bond angle changes and the displacement of the caged cation [2].

There are two orthorhombic structures, which coexist at room temperature, belonging to the *Pnma* space group. One of these structures is an edge-connected one-dimensional (1D) double-chain crystal (Y), which is yellow in color and has an indirect band gap of 2.6 eV. The other structure is a corner-linked 3D perovskite (Bγ), discovered by Yamada *et al.* [3] in 1991, which is black in color and has *p*-type conductivity with a direct band gap of 1.3 eV. When exposed to air or organic solvents, the Bγ phase undergoes a reconstructive phase transition to the Y phase under ambient conditions.

Above room temperature, two higher-symmetry structures are observed. When heated above 425 K, the Y phase transforms to a black cubic Bα phase, with the $Pm\overline{3}m$ space group. It was demonstrated by thermal analysis and x-ray diffraction (XRD) that during cooling the Bα structure deforms to a tetragonal (Bβ) structure ($P4/mbm$ space group) at 426 K [4]. On further cooling, the Bβ converts back to the Bγ phase at 351 K [1,3]. The crystal structures of the four phases are shown in Fig. 1.

The majority of the low-symmetry perovskite phases can be derived from the high-symmetry cubic structure (known as aristotypes) [5] by rigid tilting of the octahedral units around one or more of their symmetry axes, maintaining both the regularity of the octahedra and their corner connectivity [5]. Hence, the equilibrium position of the Cs atom can be thought of as being determined by the position and tilting of the SnI$_6$

octahedra for a given set of bond angles [2]. The tilting of the octahedra can be interpreted in terms of lattice-vibrational modes, with those giving rise to obvious tilt systems corresponding to some of the most important modes associated with the phase transitions in the system [6]. Based on a group-theoretical analysis employing Glazer's notation [6] and the Landau theory of phase transitions, Howard and Stokes [5] defined the group-subgroup relationships among the 15 possible space groups resulting from octahedral tilting. The order of the phase transition was identified by expressing the order parameter as a linear combination of basis functions defining a particular tilt system.

Based on this work, the $Pm\overline{3}m \rightarrow P4/mbm$ space group transition (which will correspond to the B$\alpha \rightarrow$ Bβ transition in the present study) was identified as being a continuous second-order transition, in which one rotation occurs about the c axis [5,7]. The $P4/mbm \rightarrow Pnma$ transition (corresponding to the B$\beta \rightarrow$ Bγ transition) was similarly characterized as being second order.

The unusual properties of the various CsSnI$_3$ phases, in particular the low-temperature Bγ polymorph, have attracted interest for a variety of applications. Its optical properties make it useful for light-emitting diodes, particularly as it is soluble in certain organic solvents, and can therefore be deposited on substrates or inside porous structures by solution processing [8]. Also, its strong luminescence and large optical absorption coefficient at shorter wavelengths make it suitable for photovoltaics, and high efficiency has been observed for solar-cell applications [1,8]. It is a viable Pb-free alternative to the hybrid halide perovskite CH$_3$NH$_3$PbI$_3$ [9–14]. In addition, its high hole mobility, due to the small hole effective mass, make it an excellent solid-state replacement for the electrolyte in dye-sensitized solar cells [15]. The cubic phase of CsSnI$_3$ also has interesting structural and optical properties, with high absorption coefficients at infrared, visible, and ultraviolet wavelengths, making it useful for optical and optoelectronic applications working within this range of the electromagnetic spectrum [16].
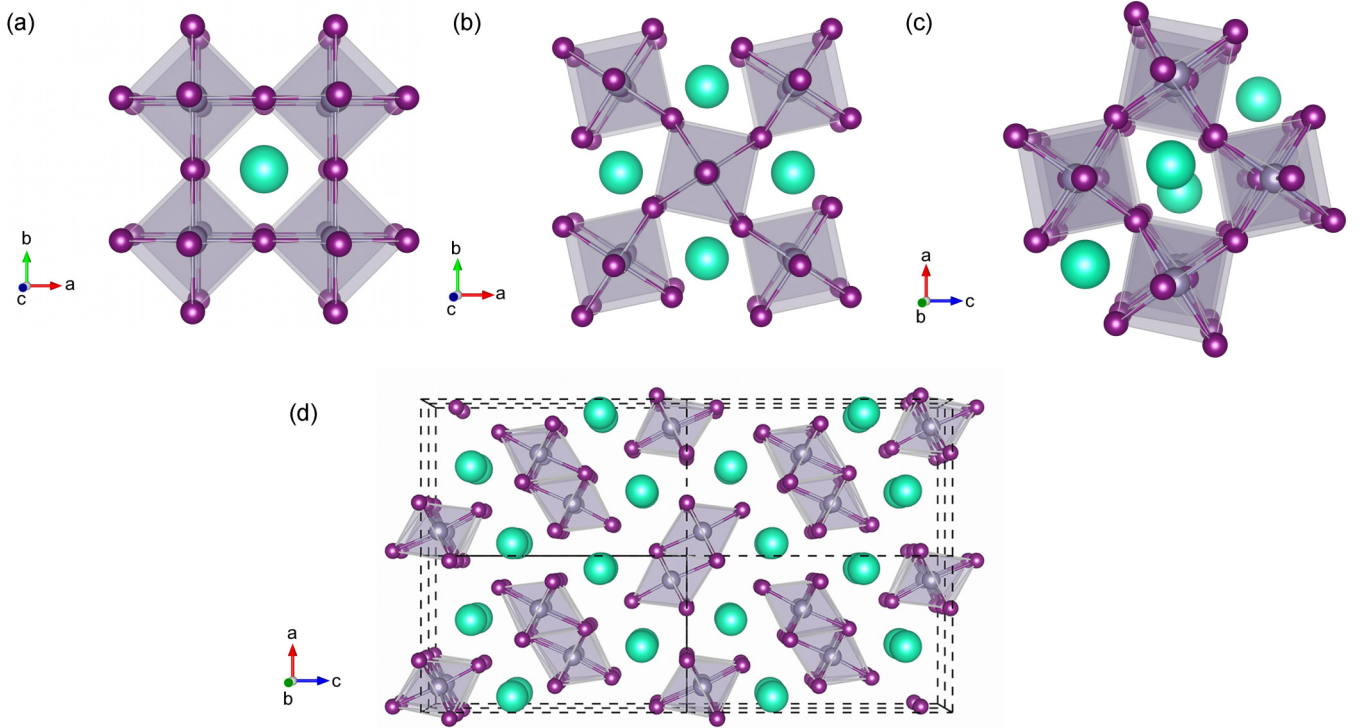
_____

[*]a.walsh@bath.ac.uk

FIG. 1. (Color online) The four polymorphs of CsSnI$_3$. On the top row, the three black perovskite structures are shown: (a) cubic Bα, (b) tetragonal Bβ, and (c) orthorhombic Bγ. The bottom row shows the yellow crystal where the tin halide octahedral networks are fragmented into one-dimensional chains (d). In all four images, the green spheres represent the Cs atom, while the purple polyhedra represent the octahedral perovskite cage formed by the bonding of the Sn (steel blue) and I (dark purple) atoms.

By exploring the Cs position offsets and lattice expansion [2], it has been predicted that the Bα structure is never an energy minimum, and can be deformed to the Bβ state without any energy barriers [2]. The structural transition between the Bβ and Bγ phases is also expected to be reversible with temperature [2]. However, the Bα and Bβ phases are both high-temperature structures, and, according to Ref. [7], the phase transitions are related to soft-mode displacements. The temperature dependence of the phonon frequencies of the four structures, and the corresponding effect on the crystal entropy and free energy, are thus likely to play an important role in defining the phase equilibria; these effects are not taken into account through the internal lattice energies of the system obtained from athermal electronic-structure calculations.

Over the past year, many studies have been carried out on CsSnI$_3$, focusing mainly on characterizing the phase transitions between the black and yellow forms. In particular, recent work carried out by Huang and Lambrecht [7] has provided a more fundamental view of the phase equilibria in CsSnI$_3$, identifying the soft phonon modes which underpin the transformations between them.

In the present work, we perform quasiharmonic lattice-dynamics calculations to characterize the temperature dependence of the properties of the four phases of CsSnI$_3$, focusing in particular on the form of the phonon dispersions and the relative Gibbs free energy. When mapping out the free energy as a function of temperature based on the 0 K equilibrium structure, the lattice vibrations are modeled as independent harmonic oscillators, and the constant-volume (Helmholtz) free energy is defined as a sum of the lattice energy and the (temperature-

dependent) vibrational contribution from the population of the phonon energy levels [17]. However, variation in the lattice volume due to thermal expansion/contraction leads to changes in both the lattice energy and the phonon frequencies, which causes a temperature dependence of the thermodynamic potentials. These anharmonic effects, which are taken into account in the quasiharmonic approximation (QHA), may be required to reproduce the subtleties of the free-energy landscape. The calculations also yield structural properties as a function of temperature, giving a first-principles estimate of the temperature dependence of the lattice volume, thermal-expansion coefficient, and other thermoelastic properties.

II. QUASIHARMONIC APPROXIMATION

In statistical physics, the Helmoltz free energy, F, is defined in terms of the canonical partition function, Z, by the so-called bridge relation:

$$F = -k_{\text{B}} T \ln Z, \quad (1)$$

where k_{B} is the Boltzmann constant and T the temperature. Z defines the partitioning of energy among the energy levels associated with the degrees of freedom of the system [17,18], and for a solid is given by:

$$Z(T) = \exp(-\phi/k_{\text{B}}T) \prod_{\mathbf{q},\nu} \frac{\exp\left[-\hbar\omega(\mathbf{q},\nu)/2k_{\text{B}}T\right]}{1 - \exp\left[-\hbar\omega(\mathbf{q},\nu)/k_{\text{B}}T\right]}, \quad (2)$$

where ϕ is the potential energy of the system, and the product runs over vibrational modes ν and reciprocal-space

wave vectors **q**, with the phonon occupation number for each mode obtained from a Bose-Einstein distribution using the characteristic oscillator frequency ω. [18,19]

The temperature-dependent Helmoltz free energy is hence given by [20]:

$$F(V,T) = \phi + \frac{1}{2} \sum_{\mathbf{q},\nu} \hbar\omega(\mathbf{q},\nu)$$
$$+ k_{\mathrm{B}}T \sum_{\mathbf{q},\nu} \ln\{1 - \exp[-\hbar\omega(\mathbf{q},\nu/k_{\mathrm{B}}T)]\} \quad (3)$$

with $\hbar$ being the reduced Planck constant. The second term is a sum of the modal contributions to the zero-point vibrational energy, and the third term is the contribution of each mode to the free energy due to thermal occupation of the phonon energy levels.

Phonon frequencies are derived from the restoring force in response to the displacement of ions by a small amplitude from their equilibrium positions. The interatomic force constants (IFCs) can either be computed from perturbation theory (e.g., density-functional perturbation theory), or by performing force calculations on a series of symmetry-inequivalent displaced structures and fitting the force/displacement curves to a harmonic function. In the latter finite-displacement (direct) method, the Parlinski-Li-Kawazoe supercell approach is commonly employed [21,22] to capture the long-range contributions to the IFCs between atoms in different crystallographic unit cells, which are needed to accurately calculate the frequencies of short-wavelength phonon modes [19].

In the harmonic model, the equilibrium distance between atoms is independent of temperature. The anharmonic effects needed to account for thermal expansion can be introduced by the QHA, in which the thermal expansion of the crystal lattice is obtained from the volume dependence of the phonon frequencies. The evaluation of the equilibrium volume and Gibbs free energy at a temperature T is obtained by minimising the function $F(V,T)$ for a given (constant) pressure p [17,20]:

$$G(T,p) = \min_{V}[F(V,T) + pV], \quad (4)$$

where $\min_{V}$ means that for each value of T and p, the function is minimized with respect to volume.

To perform a QHA calculation, the phonon frequencies are computed for a range of expansions and compressions about the 0 K equilibrium volume, and the constant-volume free energy for each calculation is evaluated as a function of temperature. From this approach, the equilibrium volume, bulk modulus, and Gibbs free energy can be obtained at arbitrary temperatures by fitting the free energy as a function of volume to an equation of state [23,24]. The temperature dependence of various derived properties, e.g., volumetric expansion coefficients and the mean Grüneisen parameter, are then readily obtained.

The mode Grüneisen paramaters, $\gamma_{\mathbf{q},\nu}$, quantify the change in each phonon frequency with volume V through [25,26]:

$$\gamma_{\mathbf{q},\nu} = -\frac{V}{\omega_{\mathbf{q},\nu}}\frac{\partial\omega_{\mathbf{q},\nu}}{\partial V} = -\frac{\partial\ln\omega_{\mathbf{q},\nu}}{\partial\ln V}. \quad (5)$$

These are related to the temperature-dependent mean Grüneisen parameter by:

$$\gamma = \sum_{\mathbf{q},\nu}\frac{C_{\mathbf{q},\nu}\gamma_{\mathbf{q},\nu}}{C_{\mathrm{V}}}, \quad (6)$$

where C_{V} is the constant-volume heat capacity, and $C_{\mathbf{q},\nu}$ are the contributions from individual modes:

$$C_{\mathbf{q},\nu} = \hbar\omega_{\mathbf{q},\nu}\frac{\partial n(T,\omega_{\mathbf{q},\nu})}{\partial T} \quad (7)$$

with $n(T,\omega_{\mathbf{q},\nu})$ being the phonon occupation number.

Within the QHA, the mode Grüneisen parameter [and, by Eq. (6), the mean Grüneisen parameter] is related to the volumetric thermal expansion coefficient, α_{V}, according to:

$$\alpha_{\mathrm{V}} = \frac{\partial\ln V}{\partial T} = \frac{1}{BV}\sum_{\mathbf{q},\nu}C_{\mathbf{q},\nu}\gamma_{\mathbf{q},\nu}, \quad (8)$$

where B is the (temperature-dependent) bulk modulus.

When the mean Grüneisen parameter γ is negative, α_{V} will likewise be negative, indicating negative thermal expansion (NTE), i.e., a reduction in volume upon heating [25,27,28]. NTE behavior in bulk systems has been linked to a number of microscopic mechanisms, including, among others, ferroelectric, magnetostrictive, and displacive phase transitions, low-frequency phonon modes and rigid-unit modes [27].

III. COMPUTATIONAL METHODOLOGY

Electronic-structure calculations were performed within the density-functional theory (DFT) [29,30] framework, as implemented in the Vienna *Ab initio* Simulation Package (VASP) code [31–33]. The semilocal generalized-gradient approximation functional with the Perdew-Burke-Ernzerhof parametrization revised for solids (PBEsol) [34,35] was employed for all the calculations. Projector augmented-wave (PAW) [36,37] pseudopotentials were used to treat semi-core electronic states, with the $Cs[5s^25p^66s^1]$, $I[5s^25p^5]$ and $Sn[5s^25p^2]$ electrons being treated as valence states.

The starting point for our calculations was a full structural relaxation of the four phases, performed with a plane-wave kinetic-energy cutoff of 800 eV. Such a high cutoff was found necessary to converge the phonon dispersion curves (see Appendix A). The Brillouin zone (BZ) was sampled with Γ-centered Monkhorst-Pack meshes [38] with subdivisions of Bα: $8\times8\times8$; Bβ: $8\times8\times9$; Bγ: $6\times5\times6$; and Y: $4\times6\times3$.

Equilibrium volumes, lattice parameters, and bulk moduli were determined by fitting energy-volume curves to the Birch-Murnaghan equation of state [23,39] (Table I). The lattice parameters obtained in the present calculations are slightly underestimated with respect to the experimental data, which, assuming positive thermal expansion, is expected, given that these are 0 K values, whereas the experimental parameters are recorded at finite temperature [19]. The Sn-I and Cs-I bond lengths in the optimized structures are tabulated in Table II.

We also calculated the heats of formation of the four phases of $CsSnI_3$ with respect to the constituent elements in their standard states Table III; additional electronic-structure calculations were therefore carried out on the published crystal structures of Cs ($Im\bar{3}m$), Sn ($I4_1/amd$), and I ($Cmca$) [40],

TABLE I. Equilibrium volumes, lattice parameters, and bulk moduli of the four different polymorphs of $CsSnI_3$, determined by fitting to the Birch-Murnaghan equation of state [23,39]. Experimental values obtained from Ref. [1] are given in parentheses. Experimental measurements of B_0 were not available for the Bα, Bβ, and Y phases for comparison.

	V ($\mathring{A}^3$)	a_0, b_0, c_0 ($\mathring{A}$)	B_0 (GPa)
Bα	230.39	$a_0 = 6.13$	18.33
		($a_0 = 6.21, \ T = 500$ K)	
Bβ	453.03	$a_0 = 8.61, c_0 = 6.11$	17.45
		($a_0 = 8.72 \ c_0 = 6.19, \ T = 380$ K)	
Bγ	897.84	$a_0 = 8.59, b_0 = 12.24, c_0 = 8.54$	15.92
		($a_0 = 8.69, b_0 = 12.38, c_0 = 8.64, \ T = 300$ K)	(19.84, $T = 300$ K)
Y	854.65	$a_0 = 10.28, b_0 = 4.73, c_0 = 17.57$	13.07
		($a_0 = 10.35, b_0 = 4.76, c_0 = 17.68, \ T = 300$ K)	

using the same pseudopotentials and plane-wave cutoff as in the $CsSnI_3$ calculations, in order to obtain reference total energies. **k**-point convergence tests were performed for all three systems, which indicated Γ-centered meshes with $26 \times 26 \times 26$, $32 \times 32 \times 34$, and $16 \times 14 \times 16$ subdivisions for Cs, Sn, and I, respectively, to be suitable.

Lattice-dynamics calculations were carried out using the supercell finite-displacement method implemented in the PHONOPY package [41,42], with VASP used as the force-constant calculator [22]. Force evaluations were performed on $2 \times 2 \times 2$ supercells using reduced **k**-point sampling meshes of $4 \times 4 \times 4$, $4 \times 4 \times 5$, $3 \times 2 \times 3$, and $2 \times 4 \times 2$ for the Bα, Bβ, Bγ, and Y phases, respectively. The phonon frequencies were sampled on an interpolated $48 \times 48 \times 48$ **q**-point mesh for the two high-temperature phases; due to the lower symmetries and larger primitive cells of the orthorhombic structures, the phonon frequencies for these were sampled on a $24 \times 24 \times 24$ **q**-point mesh.

In order to correct for the long-range Coulomb interaction, which leads to a frequency splitting of the longitudinal and transverse optic modes at the zone center (LO-TO splitting), a nonanalytical correction, based on the Born effective-charge tensors and the electronic-polarization component of the macroscopic static dielectric tensor, was applied when computing the phonon band dispersions [43]. These quantities were obtained by employing the density-functional perturbation theory routines implemented in VASP [44], with calculations being performed on single unit cells of the four structures. Convergence of these quantities required increasing the **k**-point mesh to $16 \times 16 \times 16$, $10 \times 10 \times 11$, $10 \times 9 \times 10$, and $6 \times 8 \times 5$ for the Bα, Bβ, Bγ, and Y phases, respectively.

IV. RESULTS AND DISCUSSION

A. Phase stability

To assess the relative enthalpic stabilities of the four phases, we calculated the heat of formation of $CsSnI_3$ with respect to the constituent elements according to the following:

$$\Delta H_f = E_{\text{tot}}^{CsSnI_3} - \left[E_{\text{tot/atom}}^{\text{Cs}} + E_{\text{tot/atom}}^{\text{Sn}} + 3E_{\text{tot/atom}}^{\text{I}} \right], \quad (9)$$

where $E_{\text{tot}}^{CsSnI_3}$ is the total energy (per formula unit) of the different polymorphs of $CsSnI_3$, and $E_{\text{tot/atom}}^{\text{Cs/Sn/I}}$ is the total energy per atom of the pure components in their standard states. The calculated heats of formation are tabulated in Table III; we note that neither experimental nor theoretical data was available for comparison, and thus we were unable to compare our values with other results.

The data in Table III suggest that the Y phase is enthalpically the most stable, followed closely by the Bγ and then the Bβ phases, whereas the cubic Bα phase is the least stable. This trend is consistent with the temperature ordering of the phases, and can be interpreted in terms of the relative sizes of the ions. When the ionic radii do not allow for optimal cation-halide bond lengths, it becomes energetically more favorable to displace the caged ions from their cubic positions, leading to the different distorted perovskite structures [45].

The Goldschmidt tolerance factor, t [46], for $CsSnI_3$ has been calculated to be 0.9 [7]. t is an indicator for the stability and distortion of crystal structures based on Shannon ionic radii [47], and since $t < 1$, it is expected that rotations would occur in order to stabilize the A cations in the interstitial environment, since the Sn-I cages are too big to accommodate the Cs atoms with optimal bonding. This trend is consistent with that found among the oxide perovskites, where the systems undergo transitions to the $Pnma$ space group [7].

TABLE II. Unique bond lengths in the 0 K equilibrium structures of the four different phases of $CsSnI_3$. Values are given in $\mathring{A}$.

	Sn-I	Cs-I
Bα	3.065	4.334
Bβ	3.088, 3.103	3.909, 4.272, 4.801
Bγ	3.115, 3.100, 3.107	3.847, 3.869, 3.930
		4.075, 4.084
Y	3.165, 3.008, 3.199	3.908, 4.133, 3.969
	3.326, 5.347, 5.249	3.834, 3.926, 3.855

TABLE III. Heats of formation of the four polymorphs of $CsSnI_3$, calculated from the 0 K equilibrium structures. Values are given in eV per $CsSnI_3$ unit.

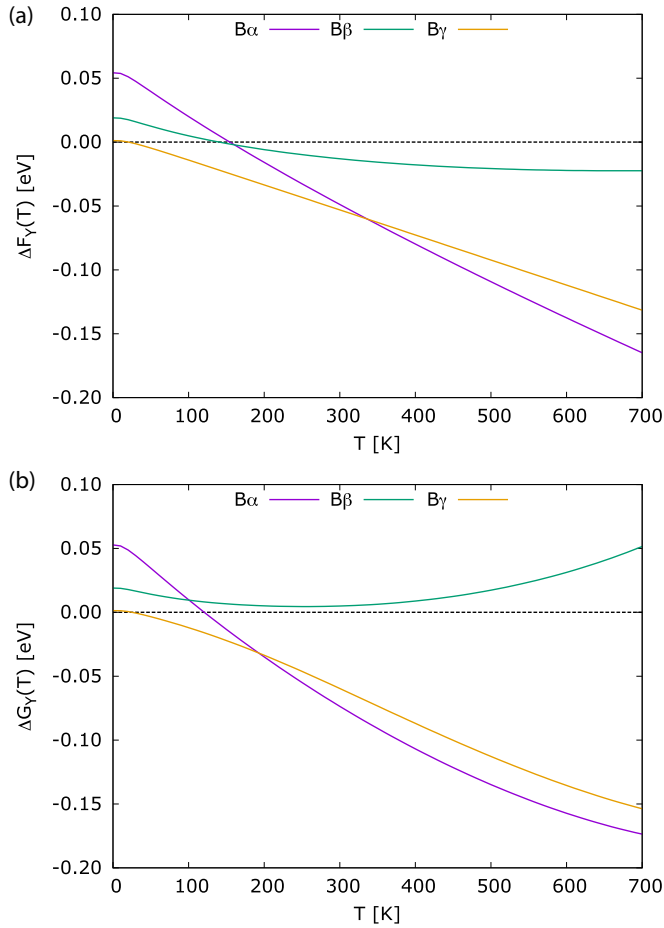| Phase	ΔH_f
Bα	-15.054
Bβ	-15.089
Bγ	-15.107
Y	-15.108

FIG. 2. (Color online) Free energy as a function of temperature for the three black CsSnI$_3$ polymorphs relative to the Y phase, which is the lowest-energy structure at 0 K. Plots (a) and (b) show the Helmoltz and Gibbs free energies, respectively. Energies are given per CsSnI$_3$ formula unit.

Within the harmonic approximation, the (Helmholtz) free energy as a function of temperature can be obtained from the phonon frequencies and lattice energy of the equilibrium structure [Eq. (3)]. By accounting for changes in the phonon frequencies due to variation in the lattice volume, the QHA calculations yield the Gibbs free energy [Eq. (4)], which is arguably more experimentally relevant. The temperature dependence of the relative (equilibrium) Helmholtz and Gibbs free energies of the four phases is compared in Fig. 2.

Both sets of data show a similar trend. At 0 K, the 1D network (Y phase) is the most stable structure, with the Bγ phase becoming favored at around 10 K. At 0 K, the cubic structure has the highest energy of the perovskite phases, and the Bγ the lowest; the energy of the Bβ phase is pinned between these competing phases. The equilibrium Helmholtz energies predict the cubic Bα phase to become stable at 300 K, transitioning directly from the Bγ phase. The corresponding transition temperature obtained from the Gibbs free energies is shifted to 200 K, but the stability trend is similar, with the Bγ structure remaining energetically close to the Bα phase up to high temperatures. These results disagree qualitatively with the electronic-structure calculations carried out by Yu *et al.* [2],

which suggested that the Bα structure can be deformed to the Bβ state without any energy barrier. This highlights the importance of taking into account contributions beyond the lattice internal energy when assessing polymorph stability.

According to our results, the Bβ phase is never more stable than the competing phases within the QHA. From the Helmholtz free energy [Fig. 2(a)], there is energetic competition between the Bα, Bβ, and Y structures around 200 K, at which the Bγ structure is the most stable. Above this temperature, the Bα phase lowers and the 1D crystal increases in energy with respect to the tetragonal phase. On the other hand, the Gibbs free energy [Fig. 2(b)] predicts that the tetragonal phase is always higher in energy than the Y phase, and is consistently higher in energy than all three competing phases above 100 K.

B. Temperature dependence of structural properties

The structural properties, as a function of temperature, obtained from the QHA are shown for each phase in Fig. 3. These include the mean Grüneisen parameter, $\gamma(T)$, the volumetric thermal-expansion coefficient, $\alpha_V(T)$, the temperature-dependent bulk modulus, $B(T)$, and the temperature-dependent volume (per formula unit), $V(T)$.

The thermal expansion of all three black phases shows a similar trend [Fig. 3(b)], whereby the expansion coefficients increase from 0 K before peaking at a low temperature and then decreasing. The expansion of the Bγ and Bβ phases both peak around 150 K, and remain positive at higher temperatures. On the other hand, the Grüneisen parameter [Fig. 3(a)] of the Bα phase shows a very sharp peak at low temperature and then a notable decrease at high temperatures, becoming negative at around 200 K; this correlates with a negative volumetric thermal-expansion coefficient.

The temperature-induced volume changes in the black perovskites are dependent on the stretching of the Sn-I bonds and the tilting of the SnI$_6$ octahedra. As all three structures have a similar SnI$_6$ octahedral framework, one may infer that the octahedral cages remain largely ideal (i.e., undistorted), and so the thermal expansion is accommodated primarily by changes in the volume of the cage [48]. The thermal expansion of the cubic phase is found to be smaller than that of the lower-symmetry phases, which is consistent with theoretical analysis performed on other centrosymmetric perovskites [48].

In contrast, the lower-dimensional Y crystal exhibits a markedly different thermal-expansion trend to the black perovskite structures [Fig. 3(b)]. We interpret this as being due to the composition of the Y phase being better described by the formula Cs$_2$Sn$_2$I$_6$, where the edge-sharing octahedra condense to form infinite one-dimensional double chains of Sn$_2$I$_6^{2-}$, separated by the Cs cations, leading to a denser structure [1].

Figure 3(c) shows the temperature-dependent bulk moduli of the four phases of CsSnI$_3$. The bulk modulus of the cubic phase shows an apparently remarkable increase with temperature, yielding a very large value at 500 K when compared to that obtained at the 0 K equilibrium volume [$B(500K) = 418.90$ GPa and $B_0 = 18.33$ GPa, respectively; Tables I and V]. This is clearly a spurious result, and, on investigation, appears to be an artifact of the fitting of the free-energy versus volume curves to the Vinet-Rose equation of state [24] for this phase [see Appendix C, Fig. 8(a)]. There
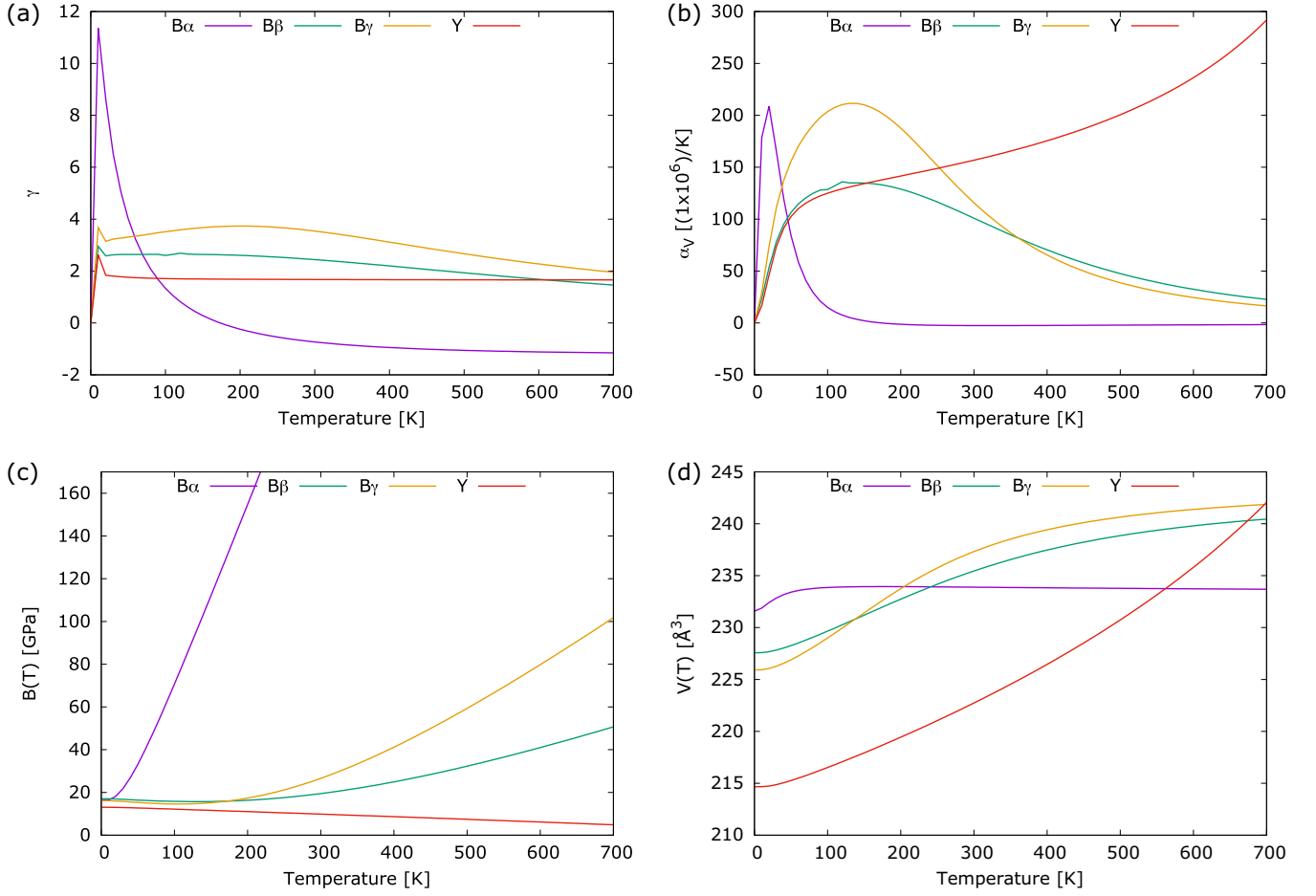
FIG. 3. (Color online) Structural properties of the four phases of CsSnI$_3$ as a function of temperature within the quasiharmonic approximation. (a) Grüneisen parameter, γ(T); (b) volumetric-expansion coefficient, α_V(T); (c) bulk modulus, $B(T)$; and (d) volume per formula unit, $V(T)$.

is a disproportionate distortion of the high-temperature free energy of the expanded structures due to the presence of the imaginary modes in the phonon density of states (see Sec. IV C).

The Bβ and Bγ phases have similar bulk moduli up to ~180 K, above which the bulk modulus of the Bγ phase increases above that of the tetragonal structure. The Y structure has the lowest bulk modulus throughout the temperature range studied. This low value is consistent with the large number of degrees of freedom, which make it a highly compressible

structure. This is likewise also reflected in the volume expansion [Fig. 3(d)] when the temperature is increased.

Table IV gives the calculated properties of the four structures of CsSnI$_3$ at the temperatures quoted in Ref. [1]. The lattice parameters are compared to values obtained from this experimental study, and are notably closer to experiment than those obtained from the 0 K equilibrium-volume calculations (Table I). We note that this is despite the apparent errors in the high-temperature bulk moduli of the cubic (Bα) phase noted previously.

TABLE IV. Structural properties of the different phases of CsSnI$_3$ at the temperatures quoted in Ref. [1] (values are shown in parentheses), calculated within the quasiharmonic approximation. γ refers to the Grüneisen parameter, and α_V is the volumetric thermal expansion coefficient.

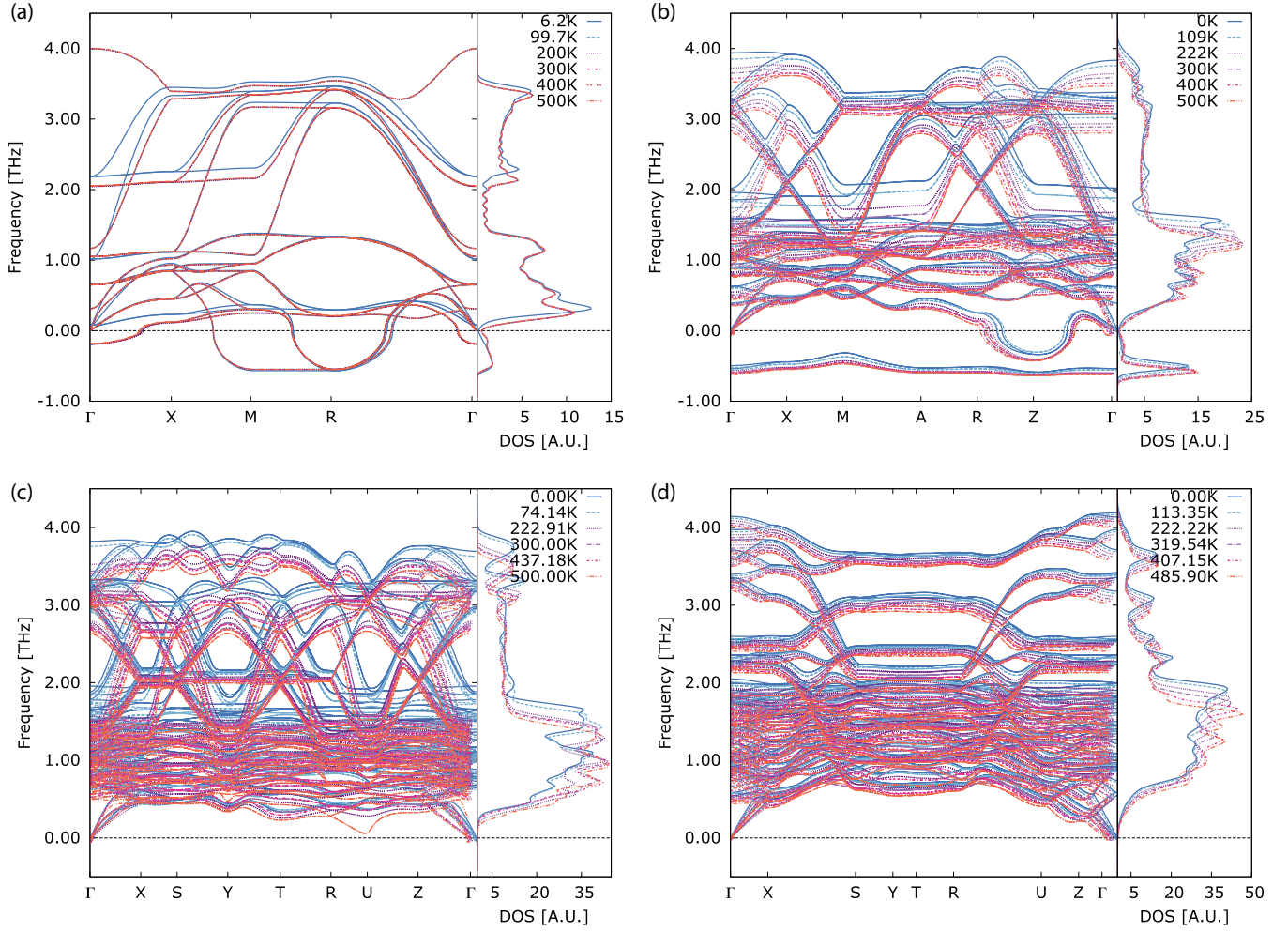|	V (Å^3)	a_0, b_0, c_0 (Å)	B_T (GPa)	γ	α_V (10^6/K)
Bα (500 K)	233.78	$a_0 = 6.16$ ($a_0 = 6.21$, $T = 500$ K)	418.90	-1.06	-2.12
Bβ (380 K)	474.24	$a_0 = 8.74$, $c_0 = 6.21$ ($a_0 = 8.72$, $c_0 = 6.19$, $T = 380$ K)	23.68	2.25	75.99
Bγ (300 K)	949.29	$a_0 = 8.89$, $b_0 = 12.41$, $c_0 = 8.60$ ($a_0 = 8.69$, $b_0 = 12.38$, $c_0 = 8.64$, $T = 300$ K)	26.59 (19.84, $T = 300$ K)	3.54	115.81
Y (300 K)	890.93	$a_0 = 10.42$, $b_0 = 4.80$, $c_0 = 17.57$ ($a_0 = 10.35$, $b_0 = 4.76$, $c_0 = 17.68$, $T = 300$ K)	9.85	1.67	156.78

FIG. 4. (Color online) Phonon dispersions and densities of states of the four different polymorphs of CsSnI$_3$, plotted for various lattice temperatures obtained from the quasiharmonic approximation (the corresponding structural parameters are listed in Table V): (a) Bα, (b) Bβ, (c) Bγ, and (d) Y. The unit cell of the Bα phase contains five atoms ($Z = 1$), whereas the Bβ unit cell is twice as large (10 atoms; $Z = 2$), and the the two orthorhombic structures both contain 20 atoms in the primitive cell ($Z = 4$).

C. Phonon density of states and band dispersion

Within the harmonic approximation, Huang and Lambrecht observed imaginary phonon modes in the equilibrium band structures of both high-temperature black phases [7]. Imaginary modes were not observed in the orthorhombic phases (Bγ and Y), indicating that the orthorhombic structures are dynamically stable at 0 K. From the temperature-dependent lattice volumes obtained in the present quasiharmonic calculations, we calculated the phonon band structures and densities of states as a function of temperature (Fig. 4; the corresponding structural parameters are listed in Table V).

As in Ref. [7], we also observe soft modes in the dispersions of the Bα and Bβ phases. In the former, the soft modes occur at the zone boundaries [**q** vectors M and R; Fig. 4(a)]. This would correspond to a phase instability due mostly to rotations of the octahedra about the crystallographic c axis [26]. From the partial phonon density of states (PDOS) of the equilibrium structure (Fig. 5), it can be seen that the main contribution to the soft modes are distortions of the perovskite cage (Sn-I), which is again consistent with the findings in Refs. [1,7]. Moreover, one must note that these zone-boundary imaginary modes do

not disappear at high temperatures (above 425 K), indicating that this structure is not dynamically stable at any of the lattice temperatures studied here.

At ~29 K, a new optic-mode instability emerges at the Γ point, corresponding to a ferroelectric phase transition, which would lead to a higher degree of disorder in the system [26]. This is similar behavior to that observed, for example, in SrTiO$_3$, where the ferroelectric phase transition occurs at low temperatures (~32 K) [26]. From the low-temperature PDOS curves [Fig. 6(a)], this disorder contribution appears to be due to the vibrations of the Cs atoms about their mean positions, which become more prominent with increasing temperature. The "rattling" motion of the Cs atom would cause the loss of the center of symmetry in the unit cell.

In support of these conclusions, Chung *et al.* [1] found that at 500 K the coordination environment and anisotropic displacement parameters (ADPs) of the Cs atoms were unusually high, and also that the ADPs of the I atoms indicated large thermal vibrations perpendicular to the Sn-I bonds, which is consistent with the distortion of the cage.

From the phonon band dispersion of the Bβ phase [Fig. 4(b)], the soft modes cross the whole of the BZ,

TABLE V. Lattice parameters of the four phases of CsSnI$_3$ at the QHA lattice temperatures at which the phonon DOS and band dispersions in Fig. 4 were obtained.

	T (K)	a_0, b_0, c_0 (Å)		T (K)	a_0, b_0, c_0 (Å)
Bα	6	$a_0 = 6.143$	Bβ	0	$a_0 = 8.622, b_0 = 6.122$
	100	$a_0 = 6.161$		109	$a_0 = 8.652, b_0 = 6.144$
	200	$a_0 = 6.162$		222	$a_0 = 8.695, b_0 = 6.174$
	300	$a_0 = 6.161$		300	$a_0 = 8.720, b_0 = 6.192$
	400	$a_0 = 6.161$		400	$a_0 = 8.745, b_0 = 6.210$
	500	$a_0 = 6.160$		500	$a_0 = 8.762, b_0 = 6.222$
Bγ	0	$a_0 = 8.609, b_0 = 12.264, c_0 = 8.559$	Y	0	$a_0 = 10.297, b_0 = 4.739, c_0 = 17.595$
	74	$a_0 = 8.633, b_0 = 12.299, c_0 = 8.583$		113	$a_0 = 10.333, b_0 = 4.755, c_0 = 17.655$
	223	$a_0 = 8.719, b_0 = 12.421, c_0 = 8.669$		222	$a_0 = 10.384, b_0 = 4.779, c_0 = 17.743$
	300	$a_0 = 8.893, b_0 = 12.410, c_0 = 8.602$		320	$a_0 = 10.436, b_0 = 4.803, c_0 = 17.831$
	437	$a_0 = 8.762, b_0 = 12.482, c_0 = 8.712$		407	$a_0 = 10.487, b_0 = 4.826, c_0 = 17.919$
	500	$a_0 = 8.792, b_0 = 12.525, c_0 = 8.741$		486	$a_0 = 10.836, b_0 = 4.749, c_0 = 17.883$

including the zone center. These soft modes persist across the temperature range studied, similar to those in the Bα phase.
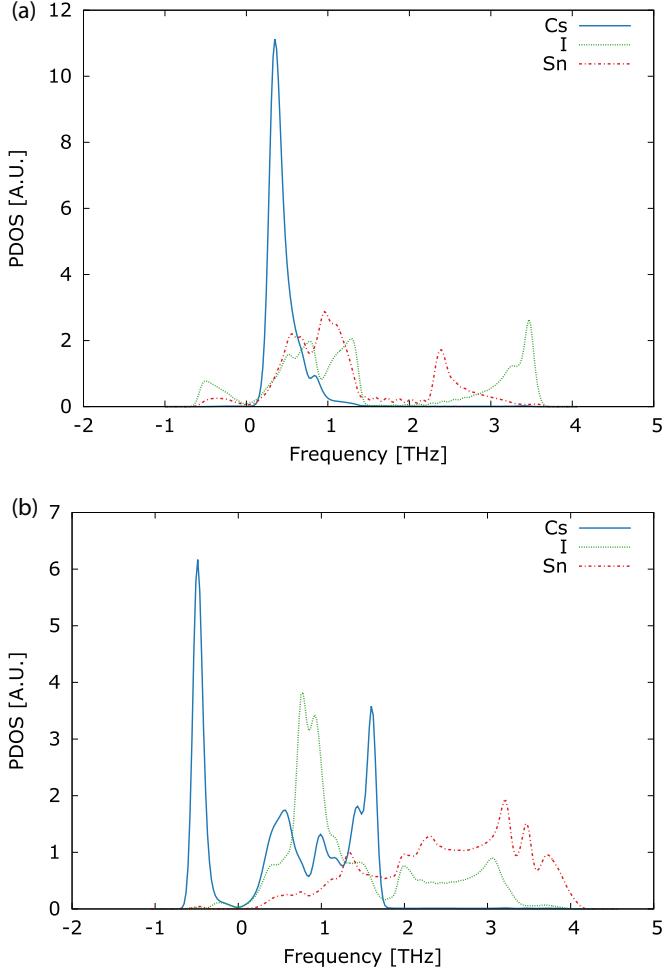
In addition, a second branch of imaginary frequencies are visible at the **q** vector Z. This is in contrast to the results in Ref. [7], where only one branch of soft modes was observed, with discontinuities along the segment M-X. We found that
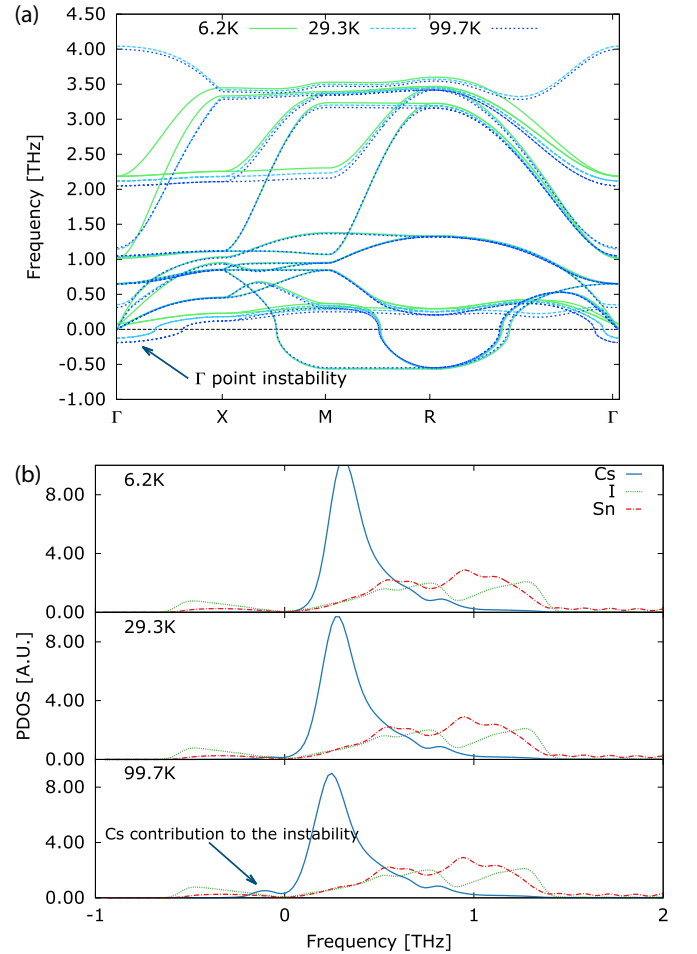

FIG. 5. (Color online) Partial phonon density of states of the Bα (a) and Bβ (b) phases of CsSnI$_3$, calculated at the 0 K equilibrium lattice parameters. It can be seen that distortions of the Sn-I cage are the major contributor to the negative part of the DOS in the Bα phase, whereas the imaginary modes in the Bβ phase are predominantly due to the motion of the caged Cs ion.

FIG. 6. (Color online) Phonon band dispersion (a) and partial density of states (b) of the Bα polymorph of CsSnI$_3$, at low temperatures. An imaginary optical mode emerges at the Γ point as the temperature increases, which appears to be due predominantly to the "rattling" of the Cs atom within the perovskite cage.

this discrepancy may be due to the different plane-wave cutoff employed in these and the other calculations (see Appendix A). In the PDOS in Fig. 5(b), the main contribution to the negative modes is the rattling of the Cs atom, with the negative-frequency part of the PDOS having a much larger amplitude on Cs than that in the Bα phase [1,7]. This effect is consistent with the instability of this system evident in the Gibbs free energy (Fig. 2), and suggests that, on cooling, structural transitions involving movement of the Cs atoms would occur [26].

The two room-temperature structures (Bγ and Y) do not show imaginary phonons over any of the temperature ranges studied in this work [Figs. 4(c) and 4(d)]. On cooling to the Bγ phase, the Cs atoms order and the structure is stable in the orthorhombic symmetry group. In this system, near 500 K a mode at the U **q** vector appears to undergo substantial softening with respect to lower-temperature structures, whereas the Y phase does not appear to show similar phenomena.

D. Discussion

We have obtained good qualitative agreement with other reports [1,7] in predicting the free-energy ordering of the different polymorphs of CsSnI$_3$, and the finite-temperature lattice parameters/cell volumes obtained from the QHA appear to be in better agreement with experimental data than those of the equilibrium (athermal) structure.

The transition temperatures estimated within the harmonic and quasiharmonic approximations are both relatively poor compared to the experimental data in Ref. [1]; for example, the transition between the Y and high-temperature cubic phases is expected to occur above 425 K, whereas the Helmoltz free-energy comparison predicts this to take place below 200 K, and the Gibbs free energies predict a transition slightly above 100 K (Fig. 2).

As the Bβ phase is not stable on the QHA free-energy landscape, these calculations predict that the Bα structure should transition directly to the Bγ phase. That said, the discrepancies between the calculated and experimentally observed transition temperatures amount to subtle energy differences, and given the apparent instability of the two high-temperature phases evident from their phonon dispersions, it is likely that these are observed as crystallographic averages of equivalent lower-symmetry structures. In this view, the transition temperatures observed experimentally would correspond to those at which sufficient thermal energy was available to allow these low-lying potential-energy maxima to be explored frequently enough to be observable in a diffraction experiment. Indeed, the Helmoltz free energy suggests that the Bα and Bγ structures are very close in energy at temperatures above ∼150 K, with the energy difference between them (∼0.02 eV) being comparable to $k_B T$ between 180 and 200 K. Similarly, the Gibbs energy difference between Bα and Bγ is around 0.01 eV between 130 and 160 K, and is roughly constant (0.02 eV) from (∼350 K) to 700 K.

It must be noted that a significant shortcoming of the present investigation is the treatment of the imaginary modes in the two high-temperature polymorphs. A proper physical description of these systems, e.g., using self-consistent phonon theory, should provide renormalized frequencies for the soft (imaginary) modes. In the present calculations, however, the

imaginary modes are excluded from the partition function when computing thermodynamic properties, whereas renormalization could produce additional low-frequency modes, which contribute significantly to the free energy. However, on inspection of the bands at explicitly calculated high-symmetry **q** points, we found that in many cases the imaginary modes were doubly or triply degenerate, meaning that an involved renormalization scheme would need to be employed, which is beyond the scope of this study. Aside from this approximation, it is also important to note that the QHA is only considered to be valid up to $\frac{2}{3}$ of the melting temperature [19], above which higher-order anharmonic effects become prominent. We would thus expect the high-temperature properties obtained from the QHA to be in error to some extent, even given an improved scheme for renormalizing the imaginary modes.

V. CONCLUSIONS

We have performed lattice-dynamics calculations within the quasiharmonic approximation on the four polymorphs of CsSnI$_3$. Our calculated structural properties suggest that, on balance, the finite-temperature lattice parameters provide a better match to experimental data than those of the equilibrium structure, despite potential issues with the treatment of
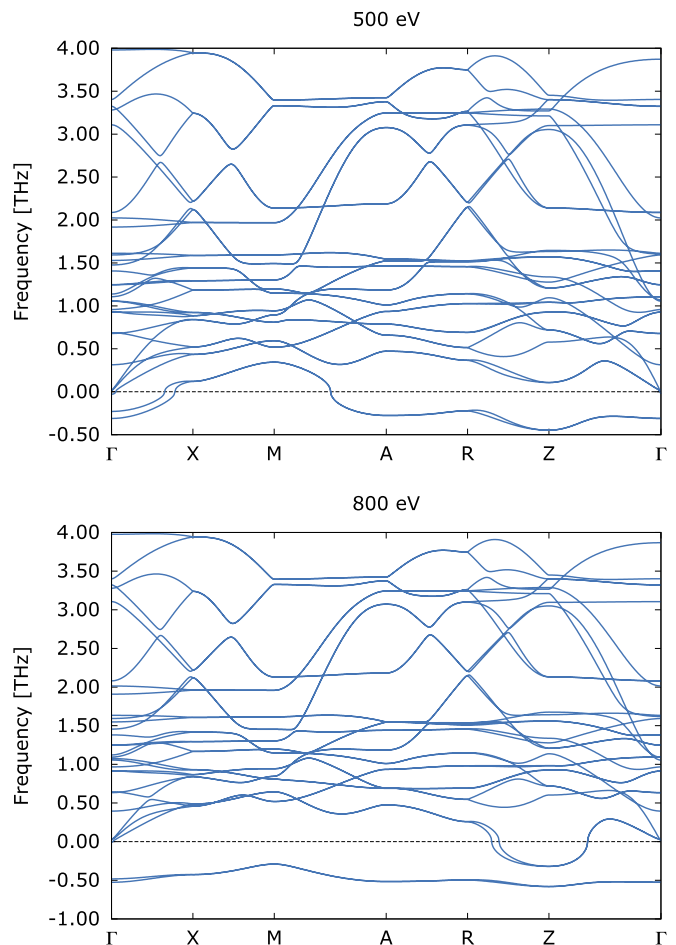

FIG. 7. (Color online) Phonon band dispersions of the Bβ phase of CsSnI$_3$ calculated with plane-wave cutoffs of 500 eV (electronically converged value; top) and 800 eV (bottom).
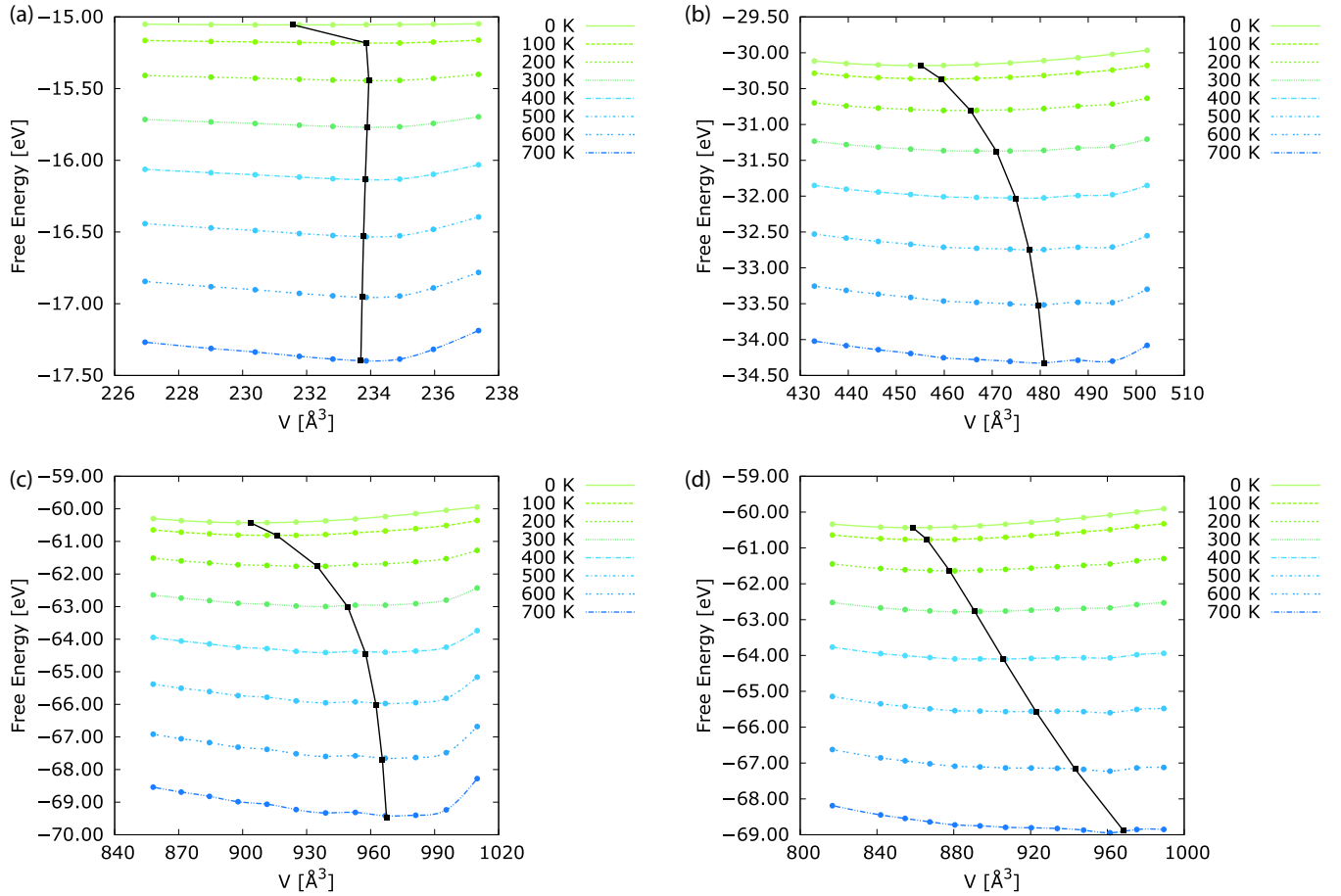
FIG. 8. (Color online) Helmoltz free-energy equation-of-state fits for the four CsSnI$_3$ polymorphs at different lattice temperatures: (a) Bα, (b) Bβ, (c) Bγ, and (d) Y. Note that the free energies are given per unit cell, and not per formula unit.

imaginary modes during the calculation of free energies. On the other hand, the predicted phase-transition temperatures do not agree quantitatively with experimental measurements, and further studies are required to pinpoint the origin of these discrepancies. From both the harmonic Helmholtz and quasiharmonic Gibbs free energies, we conclude that the Bβ phase is not stable between 0 and ~500 K with respect to competing phases. This is reflected in the calculated temperature-dependent phonon band dispersions, in which a branch of negative modes is consistently observed across the entire Brillouin zone, associated with the "rattling" of the Cs atom within the perovskite cage. The high-symmetry Bα phase also exhibits imaginary phonon modes throughout the temperature range studied, which appear to arise from motion of the Sn-I framework, and also a certain degree of disorder in the Cs atom position, evident from a zone-center ferroelectric instability which emerges at temperatures just above 0 K. On the other hand, both the ground-state phases are found to be structurally and dynamically stable, and do not show negative frequencies in their phonon dispersions up to 500 K. The significance of these findings is that the Bα and Bβ structures may be crystallographic averages over low-frequency modes in the lower-symmetry phases leading to thermal hopping between equivalent minima, and this is a point that merits further experimental and theoretical investigation. Similar behavior is expected for other tin and lead compounds in the perovskite crystal structure.

APPENDIX A: CONVERGENCE OF THE PHONON DISPERSIONS WITH RESPECT TO THE PLANE-WAVE CUT-OFF ENERGY

When carrying out DFT calculations, convergence testing is typically done based on criteria such as the total energy or stress. In the present work, we found that whereas moderate plane-wave cut-off energies (500 and 600 eV for the high-temperature and ground-state phases, respectively) were sufficient to converge the total energies and stress, a higher cutoff of 800 eV was needed to converge the phonon frequencies, in particular to eliminate artifacts at long **q**-vector regions of the phonon dispersion.

Initial harmonic-phonon calculations carried out with the lower plane-wave cutoffs gave rise to unphysical negative acoustic modes at the Γ point in calculations on the Bγ phase, indicating numerical noise in the force constants (we note that Phonopy does not symmetrize force constants by default, i.e. enforcing the acoustic-sum rule, as is a standard procedure in most codes). This issue was rectified by using a higher cutoff.

In addition, for the Bβ phase we observed differences in the low-frequency phonon modes, most notably the dispersion of the imaginary modes across the BZ, with different cutoffs (Fig. 7). When the lower cutoff was employed, negative frequencies were observed at every high-symmetry **q** vector bar the segment X-M; this is similar to the dispersion reported in Ref. [7]. However, where the energy cutoff was increased to 800 eV, the branch becomes negative through this segment, and a second negative-frequency branch emerges at Z.

APPENDIX B: CALCULATED TEMPERATURE-DEPENDENT LATTICE PARAMETERS

Table V lists the calculated lattice parameters for the different QHA lattice temperatures for which the phonon

densities of states and band dispersions are shown in Fig. 4.

APPENDIX C: FREE-ENERGY EQUATIONS OF STATE

In Sec. IV B, apparent artifacts were observed in the calculated high-temperature bulk moduli, in particular those of the cubic Bα phase. On investigation, we found that this was most likely due to anomalies in the high-temperature free-energy equations of state [Fig. 8(a)], in particular a disproportionately sharp increase in the free energy under expansion. Since this phenomenon is not as prominent at low temperature, it is likely due to the treatment of imaginary modes in the present calculations (see Sec. IV D). It is notable that a similar phenomenon is also observed for the ground-state Bγ phase, which we found is due to the appearance of soft modes under lattice expansions corresponding to very high temperatures on the QHA free-energy surface. From the results in Fig. 3(a), the calculated bulk moduli appear to be more sensitive to these issues than the lattice volumes, which, when compared to experimental data, appear to be reasonable for the high-temperature structures.

[1] I. Chung, J.-H. Song, J. Im, J. Androulakis, C. D. Malliakas, H. Li, A. J. Freeman, J. T. Kenney, and M. G. Kanatzidis, J. Am. Chem. Soc. **134**, 8579 (2012).

[2] C. Yu, Y. Ren, Z. Chen, and K. Shum, J. Appl. Phys. **114**, 163505 (2013).

[3] K. Yamada, S. Funabiki, H. Horimoto, T. Matsui, T. Okuda, and S. Ichiba, Chem. Lett. **20**, 801 (1991).

[4] K. Shum, Z. Chen, J. Qureshi, C. Yu, J. J. Wang, W. Pfenninger, N. Vockic, J. Midgley, and J. T. Kenney, Appl. Phys. Lett. **96**, 221903 (2010).

[5] C. J. Howard and H. T. Stokes, Acta Cryst. B **54**, 782 (1998).

[6] A. M. Glazer, Acta Cryst. B **28**, 3384 (1972).

[7] L.-Y. Huang and W. R. L. Lambrecht, Phys. Rev. B **90**, 195201 (2014).

[8] L.-Y. Huang and W. R. L. Lambrecht, Phys. Rev. B **88**, 165203 (2013).

[9] A. Kojima, K. Teshima, Y. Shirai, and T. Miyasaka, J. Am. Chem. Soc. **131**, 6050 (2009).

[10] M. Liu, M. B. Johnston, and H. J. Snaith, Nature (London) **501**, 395 (2013).

[11] J. M. Frost, K. T. Butler, F. Brivio, C. H. Hendon, M. van Schilfgaarde, and A. Walsh, Nano Lett. **14**, 2584 (2014).

[12] F. Brivio, K. T. Butler, A. Walsh, and M. van Schilfgaarde, Phys. Rev. B **89**, 155204 (2014).

[13] A. Walsh, D. O. Scanlon, S. Chen, X. G. Gong, and S.-H. Wei, Angew. Chem., Int. Ed. Engl. **54**, 1791 (2015).

[14] J. M. Frost, K. T. Butler, and A. Walsh, APL Mater. **2**, 081506 (2014).

[15] I. Chung, B. Lee, J. He, R. P. H. Chang, and M. G. Kanatzidis, Nature (London) **485**, 486 (2012).

[16] Hayatullah, G. Murtazab, S. Muhammada, S. Naeemb, M. N. Khalidb, and A. Manzar, Acta Phys. Pol. A **124**, 102 (2013).

[17] M. Sternik and K. Parlinski, J. Chem. Phys. **123**, 204708 (2005).

[18] M. T. Dove, *Structure and Dynamics*, Vol. 12 (Oxford University Press, Oxford, 2003).

[19] J. M. Skelton, S. C. Parker, A. Togo, I. Tanaka, and A. Walsh, Phys. Rev. B **89**, 205203 (2014).

[20] A. Togo, L. Chaput, I. Tanaka, and G. Hug, Phys. Rev. B **81**, 174301 (2010).

[21] K. Parlinski, Z. Q. Li, and Y. Kawazoe, Phys. Rev. Lett. **78**, 4063 (1997).

[22] L. Chaput, A. Togo, I. Tanaka, and G. Hug, Phys. Rev. B **84**, 094302 (2011).

[23] F. D. Murnaghan, Proc. Natl. Acad. Sci. U.S.A. **30**, 244 (1944).

[24] P. Vinet, J. R. Smith, J. Ferrante, and J. H. Rose, Phys. Rev. B **35**, 1945 (1987).

[25] L. H. Rimmer and M. T. Dove, arXiv:1411.7071v1.

[26] M. T. Dove, *Introduction to Lattice Dynamics*, Vol. 8 (Cambridge University Press, Cambridge, 1993).

[27] W. Miller, C. W. Smith, D. S. Mackenzie, and K. E. Evans, J. Mater. Sci. **44**, 5441 (2009).

[28] P. Tschaufeser and S. C. Parker, J. Phys. Chem. **99**, 10609 (1995).

[29] P. Hohenberg and W. Kohn, Phys. Rev. **136**, B864 (1964).

[30] W. Kohn and L. Sham, Phys. Rev. **140**, A1133 (1965).

[31] G. Kresse and J. Furthmüller, Phys. Rev. B **54**, 11169 (1996).

[32] G. Kresse and J. Hafner, Phys. Rev. B **47**, R558 (1993).

[33] G. Kresse and J. Furthmüller, Comput. Mat. Sci. **6**, 15 (1996).

[34] J. P. Perdew, A. Ruzsinszky, G. I. Csonka, O. A. Vydrov, G. E. Scuseria, L. A. Constantin, X. Zhou, and K. Burke, Phys. Rev. Lett. **100**, 136406 (2008).

[35] J. P. Perdew, A. Ruzsinszky, G. I. Csonka, O. A. Vydrov, G. E. Scuseria, L. A. Constantin, X. Zhou, and K. Burke, Phys. Rev. Lett. **102**, 039902(E) (2009).

[36] G. Kresse and D. Joubert, Phys. Rev. B **59**, 1758 (1999).

[37] P. E. Blöchl, Phys. Rev. B **50**, 17953 (1994).

[38] H. J. Monkhorst and J. D. Pack, Phys. Rev. B **13**, 5188 (1976).

[39] F. Birch, Phys. Rev. **71**, 809 (1947).

[40] R. W. G. Wycoff, *Crystal Structures 1*, 2nd ed. (Interscience Publishers, New York, 1963).

[41] A. Togo, F. Oba, and I. Tanaka, Phys. Rev. B **78**, 134106 (2008).

[42] A. Togo, L. Chaput, and I. Tanaka, Phys. Rev. B **91**, 094306 (2015).

[43] P. Y. Yu and M. Cardona, *Fundamentals of Semiconductors: Physics and Materials Properties* (Springer-Verlag, Berlin, 1996), p. 104.

[44] M. Gajdoš, K. Hummer, G. Kresse, J. Furthmüller, and F. Bechstedt, Phys. Rev. B **73**, 045112 (2006).

[45] L. Topor, A. Navrotsky, Y. Zhao, and D. J. Weidner, J. Solid State Chem. **132**, 131 (1997).

[46] V. M. Goldschmidt, Naturwissenschaftenen **14**, 477 (1926).

[47] R. D. Shannon, Acta Cryst. A **32**, 751 (1976).

[48] Y. Zhao and D. J. Weidner, Phys. Chem. Miner. **18**, 294 (1991).